Simulating the impact of glaciations on continental groundwater flow systems: 2. Model application to the Wisconsinian glaciation over the Canadian landscape

J.-M. Lemieux,[1] E. A. Sudicky,[1] W. R. Peltier,[2] and L. Tarasov[3]

Received 30 October 2007; revised 21 May 2008; accepted 5 June 2008; published 16 August 2008.

[1] A 3-D groundwater flow and brine transport numerical model of the entire Canadian landscape up to a depth of 10 km is constructed in order to capture the impacts of the Wisconsinian glaciation on the continental groundwater flow system. The numerical development of the model is presented in the companion paper of Lemieux et al. (2008b). Although the scale of the model prevents the use of a detailed geological model, commonly occurring geological materials that exhibit relatively consistent hydrogeological properties over the continent justify the simplifications while still allowing the capture of large-scale flow system trends. The model includes key processes pertaining to coupled groundwater flow and glaciation modeling, such a density-dependent (i.e., brine) flow, hydromechanical loading, subglacial infiltration, isostasy, and permafrost development. The surface boundary conditions are specified with the results of a glacial system model. The significant impact of the ice sheet on groundwater flow is evident by increases in the hydraulic head values below the ice sheet by as much as 3000 m down to a depth of 1.5 km into the subsurface. Results also indicate that the groundwater flow system after glaciation did not fully revert to its initial condition and that it is still recovering from the glaciation perturbation. This suggests that the current groundwater flow system cannot be interpreted solely on the basis of present-day boundary conditions and it is likely that several thousands of years of additional equilibration time will be necessary for the system to reach a new quasi-steady state. Finally, we find permafrost to have a large impact on the rate of dissipation of high hydraulic heads that build at depth and capturing its accurate distribution is important to explain the current hydraulic head distribution across the Canadian landscape.

Citation: Lemieux, J.-M., E. A. Sudicky, W. R. Peltier, and L. Tarasov (2008), Simulating the impact of glaciations on continental groundwater flow systems: 2. Model application to the Wisconsinian glaciation over the Canadian landscape, *J. Geophys. Res.*, *113*, F03018, doi:10.1029/2007JF000929.

1. Introduction

[2] In this paper, the numerical model developed in the companion paper [*Lemieux et al.*, 2008b] is applied to the Wisconsinian glaciation over the Canadian landscape in order to evaluate the possible impacts of the last glacial cycle on the continental groundwater flow system.

[3] The results presented in this paper are derived from the same set of simulations presented by *Lemieux et al.* [2008a]; here, however, we examine the impact of the Wisconsinian glaciation on the deep groundwater flow system across the Canadian landscape up to a depth of 10 km, while *Lemieux et al.* [2008a] focused on fluxes across the ground surface.

[4] A review of continental hydrogeology will be performed with a special focus on Canadian geological provinces as hydrogeological units. Then, the computational domain is presented followed by the climatic evolution during the last glaciation and its associated boundary conditions. The results with a discussion will be followed by the model limitations and conclusions.

2. Continental Hydrogeology

[5] Groundwater flow modeling at large-scale calls for prudent simplifications as not all geologic heterogeneities and process details affecting flow over and within the Canadian landscape can be included in the model. Commonly occurring geological materials that exhibit relatively consistent hydrogeological properties over the continent

[1]Department of Earth and Environmental Sciences, University of Waterloo, Waterloo, Ontario, Canada.
[2]Department of Physics, University of Toronto, Toronto, Ontario, Canada.
[3]Department of Physics and Physical Oceanography, Memorial University, St. John's, Newfoundland & Labrador, Canada.

0148-0227/08/2007JF000929

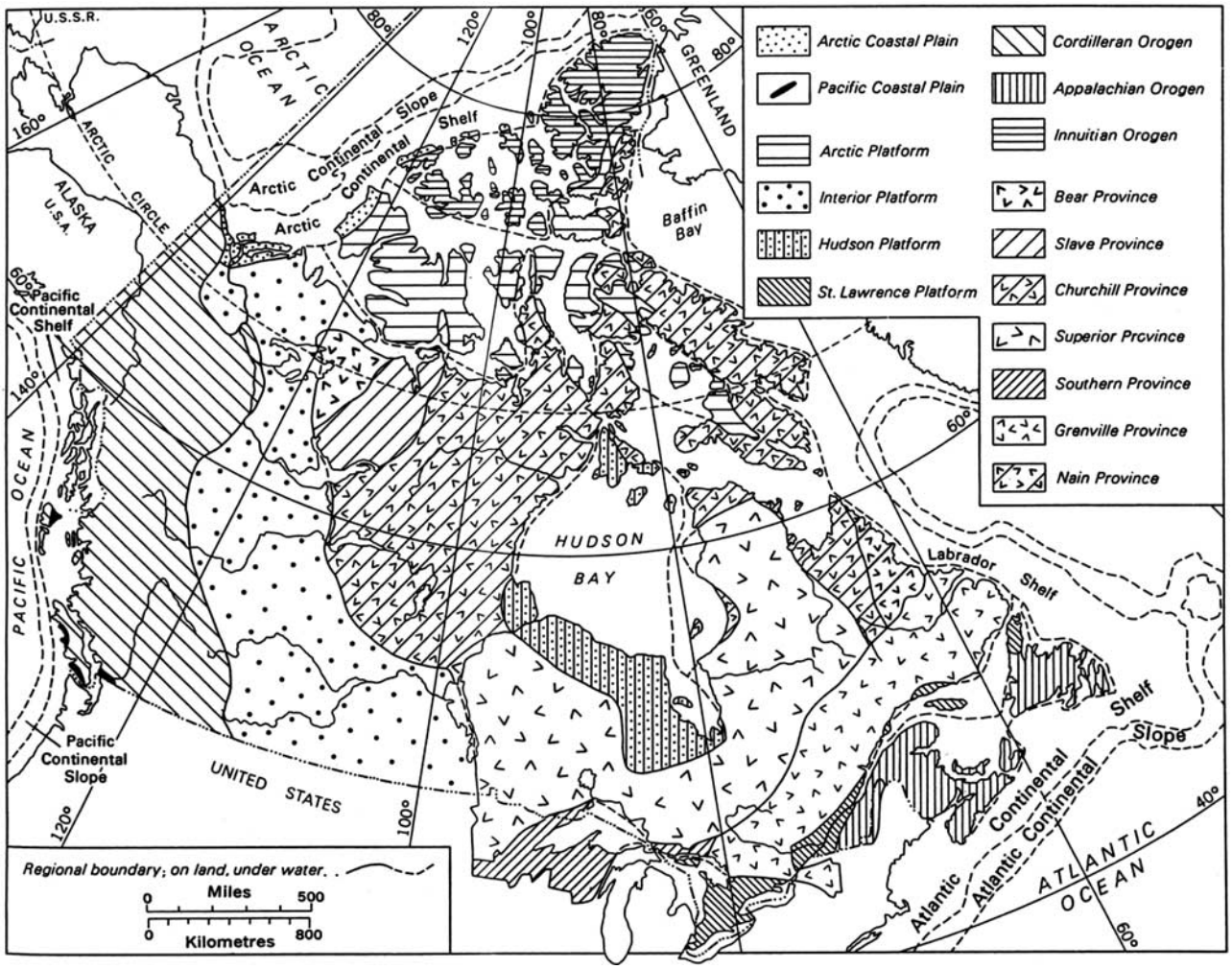

Figure 1. Geology of Canada. The Canadian Shield is made of the Bear, Slave, Churchill, Superior, Grenville, and Nain provinces. Source is *Douglas* [1970]. Reproduced with the permission of Natural Resources Canada 2008, courtesy of the Geological Survey of Canada.

can, nevertheless, enable such simplifications while still allowing the capture of large-scale flow system trends. The large time periods involved in this study requires the consideration of a wide range of climatic conditions that are usually not included in hydrogeological studies such as permafrost development, isostasy and ice loading. In this section, a review of Canadian continental hydrogeology is performed, focusing on the different geological provinces as hydrogeological units.

2.1. Bedrock Hydrogeology

[6] The geological architecture of Canada is dominated by the Precambrian Canadian Shield which forms the backbone of the continent (Figure 1). The Shield consists of several Archean fragments composed of granitic rocks and gneiss along with volcanic greenstone belts and broader tracts of sedimentary rocks [*Wheeler et al.*, 1997]. The Shield also contains younger orogenic belts between the Archean fragments made of continental, oceanic, and collisional deposits and foreign or exotic fragments.

[7] Few detailed hydrogeological studies have been performed in the Canadian Shield, and much fewer at depth, mainly because the region is sparsely populated and because the surface waters are of good quality [*Farvolden et al.*, 1988; *Rouleau et al.*, 2003]. Most of the detailed studies are related to the geological storage of radioactive nuclear wastes deep within crystalline rocks. These studies were mainly conducted in the Chalk River and Atikokan areas in Ontario and at the Underground Research Laboratory (URL) near Pinawa, Manitoba. The studies conducted at these sites indicate that the rock is fractured extensively at scales ranging from meters to tens of meters or more in terms of fracture spacings and there exist zones which can be broadly categorized as sparsely fractured, moderately fractured and highly fractured rock (e.g., *Raven* [1986] and *Stevenson et al.* [1996] among others). In general, the degree of fracturing decreases with depth from the surface. The virgin rock mass is saturated at depth [*Raven and Gale*, 1986] with the water table being commonly within a few meters of the surface in the Shield. If the fracture zones are connected in a network, then this connectivity will allow groundwater circulation even though the rock matrix has very low permeability. Because of the magmatic and metamorphic history of the rocks, the primary porosity is very low as well as its permeability. The permeability is usually much higher in the upper few tens to hundreds of meters

Table 1. Compilation of Hydraulic Properties Reported in the Literature for the Canadian Shield

Depth	Medium	Hydraulic Conductivity, K (m/a)	Specific Storage, S_s (m^{-1})	Porosity, ϕ	References[a]
Shallow (<500 m)	Matrix	10^{-5}–10^{0}			3,4
Shallow (<500 m)	Fracture	10^{-3}–10^{3}	1×10^{-5}	0.001–0.042	2,3,4
Shallow (<500 m)	Bulk	10^{-1}–10^{2}		0.027	1,5,6,7,8
Deep (>500 m)	Matrix	10^{-6}–10^{-4}			4
Deep (>500 m)	Fracture	10^{0}–10^{4}			4
Deep (>500 m)	Bulk	10^{-2}			1

[a]The references are as follows: 1 is *Raven et al.* [1987], 2 is *Raven* [1986], 3 is *Farvolden et al.* [1988], 4 is *Stevenson et al.* [1996], 5 is *Frost and Everitt* [1997], 6 is *Kuchling et al.* [2000], 7 is *Raven and Gale* [1986], and 8 is *Frost* [1997].

and significantly diminishes with depth, although there is no single relationship between depth and permeability. *Farvolden et al.* [1988] point out that a log-linear decrease can usually be observed in the first 400 m and that the deeper hydraulic conductivity values tend to be variable depending on the fractures or faults intercepted. At great depths, the permeability decreases dramatically and *Neuzil* [1995] suggests that minimal permeability should exist at depths greater than about 7 km. The permeability reduction with depth is due to increasing effective stresses and temperature-dependent diagenetic and metamorphic processes [*Ingebritsen and Sanford*, 1998].

[8] Table 1 is a compilation of the hydraulic properties measured in the Canadian Shield and reported in the literature. Most of the values reported were derived from studies related to nuclear waste disposal. The objective of these studies was to examine the suitability of rocks of low permeability to isolate radionuclides for a sufficiently long time so as to not pose a threat to human health should a release occur from an engineered repository located at depth. Therefore, plutons and batholiths (intrusive bodies) which are less fractured than the other rocks of the Shield were primarily investigated. The values presented in Table 1 are thus biased by low hydraulic conductivity values. Mine-site data, which have a long legacy of hydraulic testing, are generally not accessible because of confidentiality reasons. One of the few compilations of mine-related hydraulic measurements found in the literature is from *Raven and Gale* [1986]. Results presented in Table 1 are divided into shallow (<500 m) and deep (>500 m) measurements, and for each depth category, values are reported for the matrix, the fractures or the bulk rock mass depending on the nature of the measurements. The matrix measurements reported here are not necessarily representative of the intact rock matrix itself because the matrix can include small pervasive fractures. Nevertheless, it can be seen from Table 1 that deeper measurement locations typically exhibit a lower hydraulic conductivity. It is also clear that specific storage measurements are lacking in most published reports.

[9] *Stober and Bucher* [2005] present the results of a 1-year-duration pumping test in a pilot hole of the deep research drill hole (KTB) in the crystalline basement of central Germany in which 23,100 m^3 of saline water was extracted. The results are quite unexpected because the experiment indicated that the pore space of the upper crust is highly fractured and connected and, therefore, the continental upper crust can be considered as an aquifer. The interpretation of the pumping test data yielded a hydraulic conductivity of 4.1×10^{-8} m/s with a storage coefficient (storativity) of about 5×10^{-6} (specific storage, $S_s = 3.3 \times 10^{-8}$ m^{-1}). The average flowing porosity of the fractured rock was determined to be 0.6–0.7%. *Stober and Bucher* [2005] concluded that this range can be taken as representative and characteristic of the continental upper crust in general. A simplified cross section is shown in Figure 2 in which the continental crust is divided into an upper brittle permeable crust and a lower ductile aquiclude separated by a transition zone. The upper part of the crust is a saturated and permeable rock mass because of a connected fracture pore space [*Stober and Bucher*, 2004]. This hydrogeological conceptualization of the upper crust probably holds for the Canadian Shield, at least over the upper 10 km which is the depth range considered in the present study. This is also the depth range over which direct measurements of permeability in the crust have been conducted [*Huenges et al.*, 1997].

[10] There are three younger deformed orogenic belts across Canada, mainly consisting of Phanerozoic rocks surrounding the Shield (Figure 1). The formation of the mountains was accompanied by volcanic eruptions and metamorphism. The rocks in these belts have also undergone folding, faulting and uplift. The permeability distribution is therefore highly variable. The most dominant feature for groundwater flow is the fractures and faults that formed along with the mountains (e.g., *Randall et al.* [1988] for the Appalachians) as well as the deformed lithology (e.g., *Foxworthy et al.* [1988] for the Cordillera). Water flows mainly through the fractures under gravity drainage from the high elevations to the lower valleys.

[11] The hydraulic properties of the shallow rocks of the Appalachians were compiled by *Randall et al.* [1988]. Hydraulic conductivity values for porous and nonporous bedrock varies between 1.1×10^{-6} m/s (≈35 m/a) to 1.65×10^{-5} m/s (≈520 m/a). Specific storage values are typically near 2×10^{-2} m^{-1}. These data originate from tests conducted in industrial and municipal wells, which put a bias in the data because only the shallow regime high hydraulic conductivity values are measured in such studies. Much lower-permeable rocks, not likely to be explored in such studies, were not tested; thus the values presented above represent the upper range in values.

[12] Large parts of the Canadian Shield are covered by the Interior, Arctic, Hudson and St. Lawrence Platforms and are thin layers of undeformed sedimentary rocks, except for the Western Canada Basin (Interior Platform) east of the Cordillera. These are mainly of early Paleozoic age (Figure 1) and rest unconformably over the Canadian Shield. The St. Lawrence Platform is a Cambro-Ordovician sequence of continental to deep marine sediments, starting with sandstones at the bottom, followed upward by a carbonate platform and overlain by thick shale deposits. The beds are subhorizontal with large-amplitude gentle folds [*Globensky*, 1987]. Large faults are common across the platform and it contains a network of extensive small-scale and bed-contained fractures [*Lemieux et al.*, 2006]. Extensive

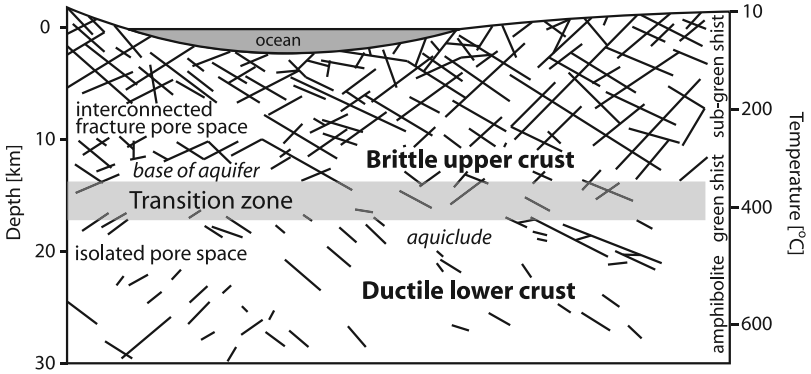

Figure 2. Schematic cross-section trough of the continental crust. Brittle upper crust with an interconnected pore space (aquifer) and lower ductile crust with isolated fractures (aquiclude) are shown. Modified from *Stober and Bucher* [2004] with permission from Blackwell publishing.

hydraulic testing of the sandstone, dolostone and carbonate rocks near Montreal is reported by *Nastev et al.* [2004]. Hydraulic conductivity values vary from 10^{-8} m/s to 10^{-3} m/s ($\approx 3 \times 10^{4}$ m/a) with an overall geometric mean of 2.6×10^{-5} m/s ($\approx$820 m/a). A weak decreasing trend of the transmissivity with depth was observed to a depth of 100 m.

[13] The Interior Platform, also referred to as the Interior Plains or Western Sedimentary Basin, lies between the Cordillera and the Canadian Shield (Figure 1). The Western Sedimentary Basin is a westward-thickening wedge of Mesozoic and Cenozoic sediments. The sediments that form the basin are a succession of sandstones, shales and carbonates. *Garven* [1989] provides hydraulic conductivity values for the main units comprising the Western Sedimentary Basin. Horizontal hydraulic conductivity values range from 0.001 to 200 m/a and vertical values range between 1×10^{-5} and 20 m/a. Specific storage coefficients range from 1×10^{-3} to $\times 10^{-5}$ m^{-1} and porosity between 0.05 and 0.3 depending on the units. The lower values correspond to a small Devonian evaporite deposit, such that average values are likely much higher.

[14] Other sedimentary platforms are the Hudson Platform that lies in the middle of Hudson Bay (Figure 1) and the Arctic platform. There is little hydrogeological information available for these basins and because their origin is similar to that of the Western Sedimentary Basin and the St. Lawrence platform, the same hydraulic properties will be used.

[15] Finally, the oceanic crust, that extends around the periphery of the North American continent, is of basaltic composition. Because of the difficulties related to hydraulic testing in this environment, there are few studies that address the permeability within the basaltic oceanic crust. Oceanic crust permeability is intimately linked to crustal formation due to vertical layering, depending on the intrusive or effusive origin of the magma, and with lateral variations from the ridge to the continent's margin [*Fisher*, 1998]. The shallowest oceanic basement is believed to be more permeable because of pillow formation and brecciation. Vertical faults are likely to be the major conduits between the permeable surface and the deeper basalts, but these vertical faults can close because of mineral precipitation as the rocks move away from the ridge. *Fisher* [1998] reports a summary of bulk permeability measurements performed using packers as part of the Deep Sea Drilling Project and the Ocean Drilling Program. The estimated permeability values range from 10^{-13} to 10^{-18} m^2 ($\approx 10^{-4}$ to 10^{1} m/a) with an average of about 10^{-15} m^2 ($\approx 10^{-1}$ m/a). The measurements are highly variable depending on the measurement technique used and the packer vertical lengths over which the measurements were performed. Larger interval measurements tend to include large-scale features such as fracture zones, faults, or other heterogeneities and these measurements tends to be more homogeneous, while small-scale measurements tend to reflect small-scale features such as individual fractures and are thus much more variable.

[16] There are several forces that are known to cause large-scale fluid migration which include topography-driven flow, free-convection flow cells driven by buoyancy forces associated with temperature and salinity, compaction, tectonic dilation/compression, chemical diagenesis, hydrocarbon generation, etc. [*Garven*, 1995]; however, as *Garven* [1995] points out, the dominant mechanism for groundwater flow in continental masses, both shallow and deep systems, is the topographic relief [*Hubbert*, 1940; *Tóth*, 1962, 1963; *Freeze and Witherspoon*, 1967]. It should be noted that these studies did not include the presence of brines at depth which are believed to strongly influence deep-seated flow systems [*Domenico and Robbins*, 1985]. The different flow mechanisms described above evolve gradually through time. For example, the Western Sedimentary Basin, in the Late Phanerozoic, was a compaction-driven basin with free convection. During the Late Cretaceous-Tertiary time, after the Rocky Mountains formed, a large flow system developed from west to east and resulted in the Pb-Zn ore district of Pine Point and the Athabasca tar sands deposits. At present day, *Garven* [1995] claims that the current flow system can be interpreted from potentiometric maps as a topographically driven-flow system even if some abnormal pressures are measured locally. Those abnormal pressures are seen as rapid erosional unloading or as the result of Pleistocene glaciations.

[17] Because the Rocky Mountains are the youngest geological province of the country and because groundwater flow, except for some minor abnormal pressures, have been interpreted as a topographically driven flow system, it is believed that most of the present-day groundwater flow system over the Canadian landscape would be driven by topography and buoyancy forces associated with brines. *Garven* [1995] provides a list of major continental systems

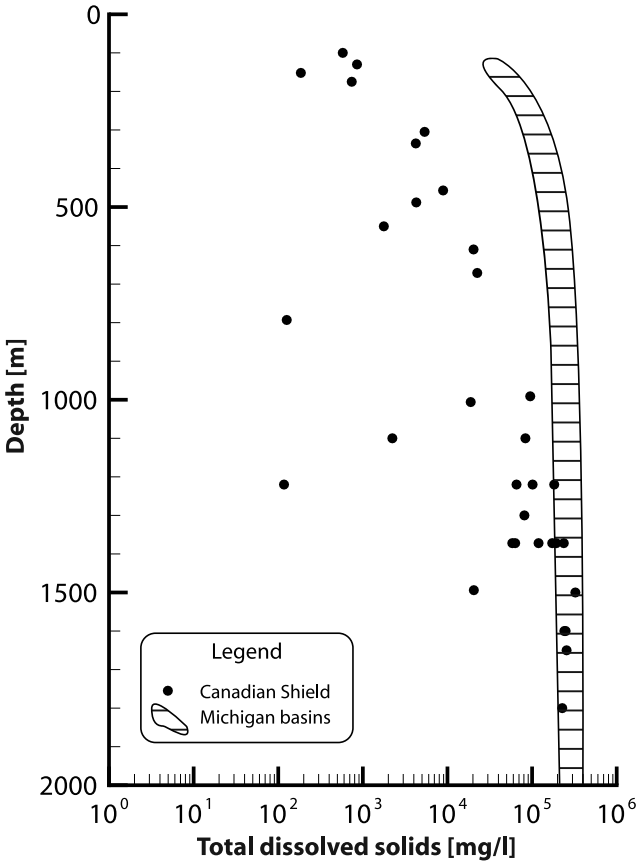

Figure 3. The relationship of depth and total dissolved solids for groundwater from the Canadian Shield and the Michigan, Illinois, and Appalachian Basins. The latest three basins are grouped together under the name Michigan Basin. Sources are *Frape and Fritz* [1987] for Canadian Shield data and *McIntosh and Walter* [2005] for the Michigan Basin data.

across the world that show chemical evidence of topographically driven flow with residence times of up to 2 Ma. These systems include the central Missouri, discharging waters from the Colorado Front Ranges, the Great Artesian Basin of Australia, the Nubian sandstone of northern Africa, Egypt, the Los Llanos Basin of Columbia and the Paraná Basin, Brazil.

[18] In Section 6, the areal and depth distribution of the various rock types and the hydrogeological properties assigned to them will be discussed further. Again, the reader should keep in mind that a high-resolution bedrock description of Canada in unavailable, at least to depths of several kilometers, and that the developed groundwater model can only be expected to capture large-scale trends in flow system evolution.

2.2. Groundwater Geochemistry

[19] The main geochemical feature of the Canadian Shield groundwaters is the occurrence of brines of a relatively uniform composition over the Shield [*Frape and Fritz*, 1987].

[20] There are two main groups of waters existing in the crystalline rocks of the Canadian Shield: shallow groundwater which reflects local climatic regimes and a second group which are the brines which exhibit a similar isotopic signature at all sites. A mixture of both members is also common. Although the brines and saline waters are usually observed at depth, there is some evidence that indicate they are discharging at the land surface at some locations [*Gascoyne and Sheppard*, 1993; *Sheppard et al.*, 1995]. The origin of the most concentrated brines located at depth is still in debate. One school of thinking is that the brines were derived from Paleozoic seawater while the other claims that the high salinity is the result of leaching of fluid inclusions or chemical reactions occurring with rock minerals.

[21] The major ions composing the brines are Ca-Na-Cl and their compositional load increases with depth (Figure 3). Because the brine composition is more or less uniform across the Shield, the linear density relationship with total dissolved solids (TDS) appears to be quite consistent across the sampling sites. The linear relationship that relates the density of the fluid, ρ, to its concentration in TDS, c (in grams per litre), is as follows: $\rho = 7.35 \times 10^{-4}\, c + 1$ [*Frape and Fritz*, 1987] and is valid for the whole range between freshwater and basin brine.

[22] In the Western Sedimentary Basin, highly saline brine is believed to originate from the evaporation of sea water during the accumulation of Paleozoic sediments in the basin [*Spencer*, 1987]. The brine is located at depth in the Devonian formation and is shifted updip to the east and north as the result of long-term basin-scale flow. The brine discharging as springs and diffuse zones at the northern and eastern margins of the basin are less saline compared to an expectation resulting from long-term basin-scale flow toward this belt. *Grasby and Chen* [2005] argue that these brines are not the result of long-term basin-scale flow, but rather are due to Pleistocene glacial meltwater that was driven downward, dissolved evaporite units, mixed with deeper basin brines, and now discharges out of the basin following the retreat of the ice sheet. This later flow system should be younger than the previous one and therefore cannot solely be used to interpret the present-day hydrodynamics of the basin because of the paleohydrogeology of the system.

[23] The water chemistry in deeper parts of the flow system has also been affected by subglacial recharge according to *Grasby et al.* [2000], *Grasby and Betcher* [2002], *Grasby and Chen* [2005], and *Ferguson et al.* [2007]. There is isotopic and chemical evidence of this interaction in some formations that are over 2000 m deep.

[24] Brine occurrence is also well-documented in the Michigan Basin and in Southern Ontario [*Dollar et al.*, 1991] as well as in the St. Lawrence Lowlands where deep brines are extracted for commercial purposes. Information is scarce regarding the groundwater chemistry of the orogenic belts. For the Appalachians, most of the bedrock is low soluble and the concentration of dissolved solids, even for deep wells, is low and rarely exceed 1000 mg/L [*Randall et al.*, 1988].

3. Computational Domain

[25] The modelled region covers a large region of the Earth's surface (Figure 4) and because HydroGeoSphere does not support spherical coordinates, a Cartesian coordi-

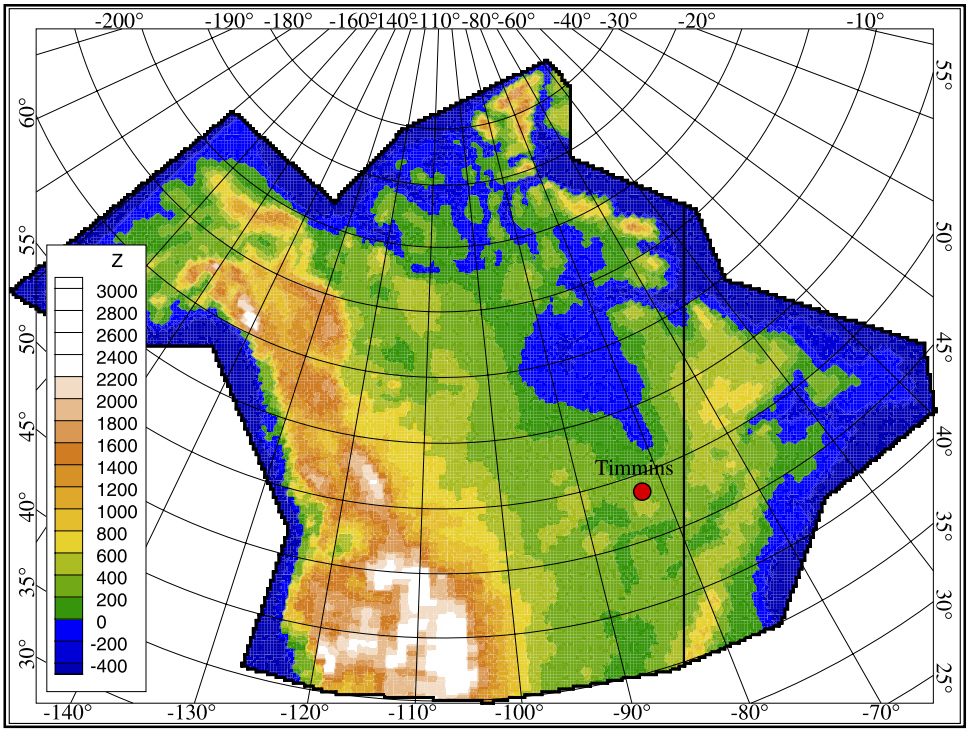

Figure 4. Limits of the numerical model. The geographic limits of the model are 172.5°W and 42.5°W on the western and eastern boundaries and 34.75°N and 84.75°N on the southern and northern boundaries. The color scale is the present-day surface elevation in m. The north-south black line indicates the location of a cross section described in section 7.

nate system was used. Map projection was used to transform geographical coordinate data sets into the Cartesian coordinate system. The Albers equal area conical projection was used because it minimizes distortion and preserves area, which means that the land masses will appear exactly the same on a terrestrial globe and on a planar surface.

[26] The limits of the model were chosen to capture the region affected by the last glaciation but are large enough such that the ice sheet impact is negligible at the margins of the model (Figure 4). Brick elements are used to discretize the model and are distributed along the principal Cartesian coordinate directions (see *Lemieux et al.* [2008a] for the discretization details). The extent of the model covers about 10,000 km × 6000 km with a total 2-D area of 2.5×10^7 km^2.

[27] The bedrock geology is simplified in the model into four major facies [see *Lemieux et al.*, 2008a, Figure 2]. Although this simplification is dramatic, computational constraints, the highly complex three-dimensional architecture of Canadian geology and the lack of systematic hydraulic measurements over the Canadian landscape limit the use of a highly-detailed geological model. The first facies is the Canadian Shield and the second includes the sedimentary basins. Average hydrogeological properties based upon a review of the hydrogeology of continental sedimentary basins are used. Most of the sedimentary basins are composed of similar types of rocks, which justifies the use of a single facies for all the sedimentary basins. The third facies is referred to as the orogen and represents the Appalachian, Rockies, and Innuitian orogenic belts. The final facies is the oceanic crust which surrounds the North American continent. The simulations performed in this study span over the last 120 ka, with a maximum time discretization of 100 a.

4. Climatic Evolution and Boundary Conditions

[28] The boundary conditions used here are inferred from the ice and climate chronologies during the Wisconsinian glaciation derived from the Memorial University of Newfoundland/University of Toronto Glacial Systems Model (GSM), as described by *Lemieux et al.* [2008a].

[29] The flow boundary conditions can be described separately for the subglacial and periglacial environments [see *Lemieux et al.*, 2008b, Figure 1]. For periglacial conditions, the assumption that the water table position equals the topographic surface elevation is made. In Canada, the water table is rarely deeper than a few meters to a few tens of meters and, given the scale of the model, it is believed that this is a reasonable assumption. The water table position is therefore specified to equal the surface elevation for all the grid nodes not covered by ice.

[30] The deformation of the crust by the ice sheet is such that the Earth's surface elevation will be depressed below the ice sheet and raised in its peripheral surroundings. The raised portion of the ground surface is referred to as the forebulge. For example, Figure 5 shows the surface elevation change in Waterloo, Ontario, Canada, for the past 120 ka.

[31] At some point, during the deglaciation period, the filling of surface depressions by glacial meltwater occurs and proglacial lakes such as lake Agassiz (−12 ka to −8 ka)

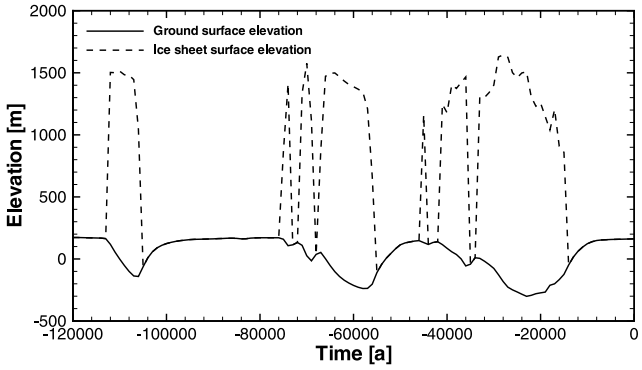

Figure 5. Ground surface and ice sheet surface elevations in Waterloo, Ontario, Canada, during the last 120 ka. The ice sheet thickness can be deducted subtracting the surface elevation from the ice sheet surface elevation.

form. In such cases, the nodes covered by lakes are assigned heads equal to the surface elevation plus the depth of the surface water bodies. The depths of these surface water bodies at 100 a time slices are available from the GSM. In some cases, the paleo-ocean level rose to levels different than a previous shore line such that a portion of the land surface was covered/uncovered by sea water. The nodes covered and uncovered by the ocean are assigned a head equal to the sea level at the value depicted by the relative sea level curve shown in Figure 6.

[32] Figure 6 shows the eustatic sea level relative to present during the last 120 ka along with the continental ice volume. These curves provide an indication of the cyclic ice sheet progression and retreat over the continent, knowing that the last glacial maximum was reached around −20 ka. Figure 6 also shows that there are three glacial maxima occurring at about −105, −60, and −20 ka, each followed by ice regressions, that are a consequence of the obliquity orbital cycle.

[33] The subglacial conditions are different depending on whether the ice sheet is cold or warm based. For warm-based conditions, a constrained specified flux is applied as described by *Lemieux et al.* [2008b]. For cold-based conditions, the same constraint is applied, but the subglacial meltwater flux is equal to zero. This allows the discharge of groundwater without exceeding the ice sheet equivalent freshwater head. Figure 7 shows the subglacial melting rate at the last glacial maximum (LGM). Meltrates in terms of water fluxes usually do not exceed a few centimeters per year except locally, near the southern margins where the meltwater rates reach about 60 cm/a. It can also be noted that the subglacial meltwater rate is quite low, or null below ice thickness maxima.

[34] The solute boundary conditions on the surface are a specified concentration equal to zero when water is entering the model, either at specified water flux or specified head nodes. A zero concentration gradient is assumed at the outlet nodes such that the solute mass can freely advect out of the domain at the resident groundwater concentration. It is believed that over the last 120 ka, the concentration will not change at a depth of 10 km below current mean sea level. Therefore, a specified concentration, c/c_{max} equal to 1.0, is specified at the bottom of the system.

[35] The boundary conditions are updated in the model at every 1 ka. For the specified head values, linear interpolation between time steps is used to obtain a smooth input function. The constraints on the specified flux are also linearly interpolated between the 1 ka time slices. Finally, Picard iteration is used to solve the nonlinear flow equation because of the variable density of the groundwater.

[36] Simulations were run on a IBM eCluster 1350 on an single 3.6 GHz processor with 8 GB of RAM. The average simulation time for the base case scenario is about 6 days.

5. Initial Conditions

[37] There is little quantitative information available concerning groundwater flow during the last interglacial. It is, however, believed that the climate during this period was similar to the current climate. This implies that the last interglacial flow system would resemble the current one. It was mentioned earlier that the current groundwater flow system can be interpreted as a topographically-driven flow system that also reflects the current boundary (i.e., climatic) conditions. By analogy, the last interglacial groundwater flow system is the result of the topography and climatic boundary conditions prevailing at that time which are provided by the GSM.

[38] A pseudo steady state simulation (i.e., a transient simulation executed until near steady state) was performed using the climatic conditions of the last interglacial. The simulation was run for 1.2 Ma before a pseudo steady state condition was achieved using time steps of 1 ka. This simulation was designed to obtain the last interglacial (LIG) flow field as well as the brine distribution. The hydraulic conductivities and the first-order brine generation source term were adjusted until the simulated TDS profiles in the Canadian Shield reasonably fit the observed profile of *Frape and Fritz* [1987].

[39] The simulated profiles of TDS are compared to the observed data for the Canadian Shield (Figure 8a) and for the Michigan Basin (Figure 8b). Although there is some discrepancy in the fit, the trend captures the increase of salinity with depth that is observed across the basins and suggests that the properties of the model are adequate.

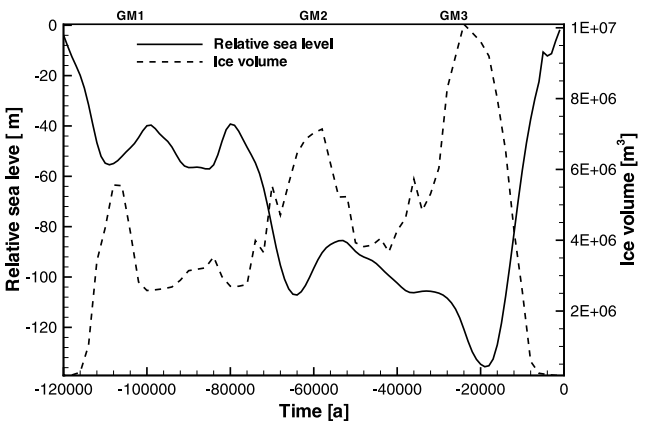

Figure 6. Relative sea level and continental ice volume during the last 120 ka. Glacial maximums are indicated with the label GM1, GM2, and GM3.

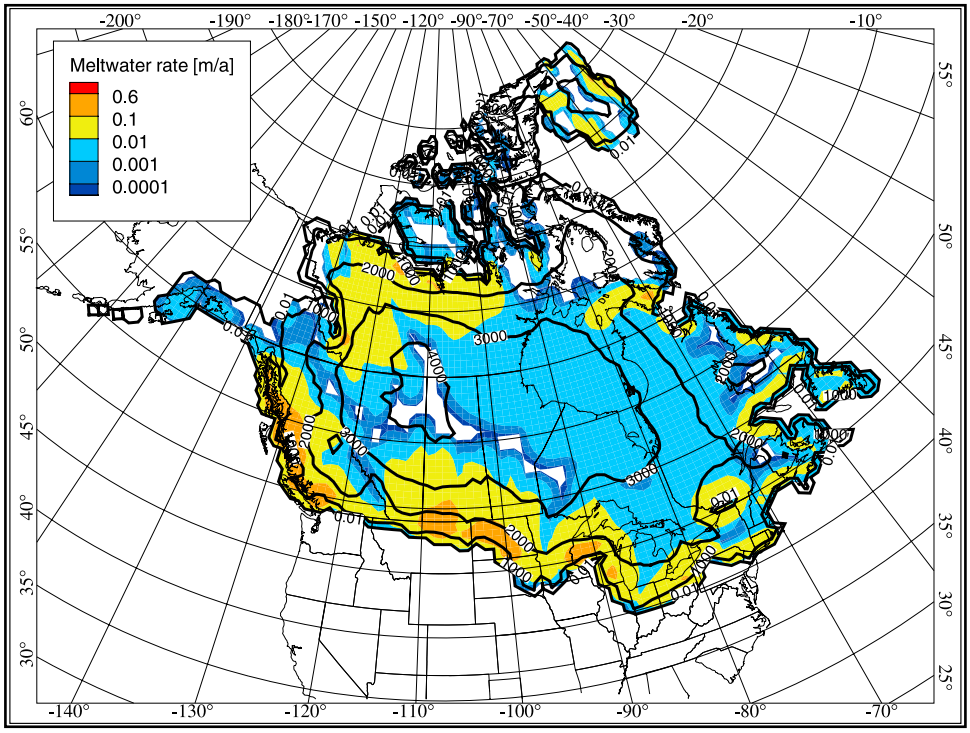

Figure 7. Subglacial meltrate (m/a) at LGM. Black contour lines represent ice sheet thickness. Source is *Tarasov and Peltier* [2004].

[40] It will be shown latter that the current groundwater flow system cannot be interpreted solely on the basis of present-day boundary conditions and it is likely that several thousands of years of equilibration time is necessary for the system to recover from the glaciation perturbation. Therefore, the initial conditions used in this model are probably partially wrong. A better approach would be to start from equilibrium, run the model through a couple of prior glacial cycles and use the end result as a starting point.

6. Input Data

[41] The surficial hydraulic properties of the four facies are provided in Table 2. The hydraulic conductivity and specific storage are assigned values on the basis of the literature review presented in Section 2.1. Obtaining a representative value for hydraulic properties for such large regions is a daunting task for several reasons. The first is because most of the studies were performed in the context of water supply which generally have a focus on relatively shallow high-permeability aquifers. The reported hydraulic properties are therefore biased but the level of bias remains unknown. The second reason is because most of the hydrogeological studies are concentrated in populated regions, which is a very small portion of Canada. The last is because the hydraulic properties of the various regions are known to be highly heterogeneous, but data are lacking to describe the spatial patterns of the heterogeneity. The values used in the model are large-scale values and implicitly incorporate large discontinuities such as fractures and faults that are likely more permeable than the host rock matrix.

[42] Because hydraulic conductivity is expected to decrease with depth because of increasing effective stresses and temperature-dependent diagenetic and metamorphic processes [*Ingebritsen and Sanford*, 1998], surface hydraulic conductivity values were reduced with depth in the model. As *Farvolden et al.* [1988] point out, the permeability reduction with depth is clearly notable over the first few hundred meters into the subsurface but deep hole measurements suggest that, at large depths, local heterogeneities may be responsible for permeability variations that mask out an unambiguous permeability reduction with depth. Alternatives to direct measurements, such as results derived from models of heat and mass transport constrained by geothermal data and the progress of metamorphic reactions driven by fluid flow, have been used to infer crustal permeability values [*Ingebritsen and Manning*, 1999]. Values estimated from these modeling studies represent large-scale estimates of a large volume of rock and are less sensitive to the scale dependance of the smaller-scale punctual measurements such as those obtained from cores and borehole measurements [*Manning and Ingebritsen*, 1999]. Permeability estimates for large and moderate crustal depths (>5 km) have been determined mainly from studies of prograde metamorphic systems, and are therefore applicable to orogenic belts where the crust is being thickened and/or heated, while lower permeabilities may occur in more stable Shield environments [*Ingebritsen and Manning*, 1999]. A relationship between depth and permeability, k, is given by $\log k = -14 - 3.2 \log z$, where k is the permeability in meters squared and z is the depth in kilometers [*Ingebritsen and Manning*, 1999] (Figure 9). The depth-permeability relationship presented by *Ingebritsen and Manning* [1999] is not appropriate for shallow environments. Therefore, for the first few kilometers of depth, a logarithmic reduction of the surface permeability is applied

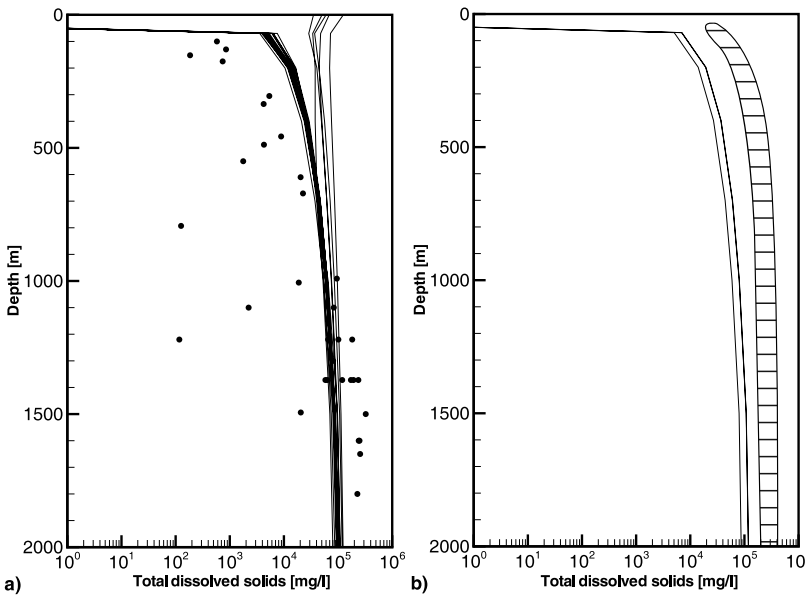

Figure 8. Simulated and observed total dissolved solids versus depth in (a) the Canadian Shield and (b) the Michigan Basin. Simulated TDS profiles are shown as continuous lines in both figures, and the observed TDS profiles are shown as circles for the Canadian Shield and as a hatched zone for the Michigan Basin.

here so as to meet the *Ingebritsen and Manning* [1999] *k-z* relationship at a tangent angle (Figure 9). The hydraulic conductivity versus depth for each rock facies is given in Figure 9.

[43] In sedimentary basins, available data suggests that the permeability distribution is more closely related to lithology than to depth. Therefore, no permeability versus depth relationship is applied to the sedimentary basins in the model. On the other hand, because of the coarseness of the model and complexity of the structure of sedimentary basins, it is not possible to include lithologic details. Instead, an average permeability value is used.

[44] It was indicated by *Lemieux et al.* [2008b] that the loading efficiency coefficient can be obtained from the elastic properties of rocks. There are no available data in the literature on values of the loading efficiency for each of the facies considered in this study. Furthermore, in low-porosity rocks, such as in the Canadian Shield, the loading efficiency is difficult to estimate because it is very sensitive to the difference between the bulk compressibility of the rock matrix and that of the solid grains, which is another unknown parameter [*Provost et al.*, 1998]. Therefore, the loading efficiency is treated as an independent and uncertain parameter in the model. For the base case scenario, a loading efficiency of 0.2 is used. Model sensitivity to this parameter is analyzed below.

[45] A series of spatially distributed time-varying data sets are derived from the glacial model and used as input. These include the surface elevation and sea level changes, ice sheet thicknesses, subglacial melting rates, lake water depths and the permafrost distribution. Updated surface elevations, ice sheet thicknesses and lake water depths are applied every 1 ka to the model with a linear interpolation between these periods in order to gradually vary the input and obtain a stable solution. The permafrost distribution, in the form of frozen elements, is also supplied every 1 ka and handled as described by *Lemieux et al.* [2008a].

[46] The dissolved solutes in the model consist of a series of anions and cations that are lumped together in the form of total dissolved solids (TDS). The maximum TDS concentration reported for groundwater is 265,000 mg/l and the fluid density at this concentration is 1262.65 kg/m^3. In the model, the fluid density is allowed to vary linearly with the concentration [see *Lemieux et al.*, 2008b, equations (11) and (12)]. The effective solute diffusion coefficient is

Table 2. Bedrock Hydraulic Properties by Facies

Parameter	Facies			
	Sedimentary	Shield	Orogen	Oceanic Crust
K (isotropic) (m/a)	60.0	30.0	3.0	0.1
Specific storage, S_s (m^{-1})	5.0×10^{-5}	3.0×10^{-6}	1.0×10^{-5}	1.0×10^{-5}
Porosity, ϕ	0.2	0.001	0.05	0.01
Loading efficiency, ζ	0.2	0.2	0.2	0.2
Longitudinal dispersivity, α_L (m)	5000	5000	5000	5000
Transverse dispersivity, α_T (m)	100	100	100	100
Transverse vertical dispersivity, α_V (m)	100	100	100	100
Rock water mass transfer constant, K_{mt} (a^{-1})	2.3×10^{-7}	2.3×10^{-8}	2.3×10^{-8}	2.3×10^{-9}

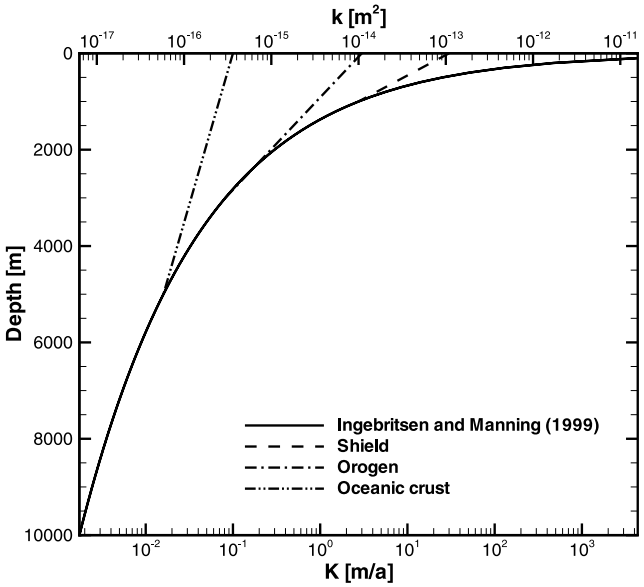

Figure 9. Hydraulic conductivity and permeability versus depth from Ingebritsen and *Manning and Ingebritsen* [1999] and for each rock facies. For illustrative purposes, hydraulic conductivity, K, is also shown (computed with water density and viscosity values at 15°C).

0.015 m^2/a and a constant fluid viscosity equal to 1.12×10^{-3}Pa was assigned to the fluid.

7. Numerical Dispersion

[47] Numerical dispersion is controlled by two factors: the grid spacing and the time step size. In one dimension, the grid spacing is constrained by the grid Peclet criterion which is given by

$$Pe = \frac{v\Delta x}{D} \leq 2, \tag{1}$$

where $v = q/\phi$ is the average pore water velocity ($L\,T^{-1}$), q is the Darcy flux ($L\,T^{-1}$), ϕ is the porosity (dimensionless), D is the dispersion coefficient ($L^2\,T^{-1}$), and Δx is the grid spacing (L). The chosen longitudinal dispersivity (5000 m) respects this criterion. The use of large values in the horizontal and transverse dispersivities are also commensurate with the large size of the finite elements and subgrid-scale heterogeneity that would promote mixing.

[48] The time step is constrained by the grid Courant criterion which is given by

$$Cr = \frac{v\Delta t}{\Delta x} \leq \frac{Pe}{2}. \tag{2}$$

With a maximum value of $Pe = 2$, the Courant criterion yields the constraint

$$\Delta t \leq \frac{\Delta x}{v}. \tag{3}$$

[49] Considering that the element sizes are on the order of kilometers in length and that the velocity does not exceed a few meters per year, except for a few short-term peaks, the selected time step of 100 a is small enough to satisfy the Courant criterion. Little numerical oscillations was observed during large subglacial infiltration events (see Figure 11e), but the overall stability of the model was satisfactory and converging rapidly at every time step.

8. Results

[50] Before examining the impact of the glacial cycle on continental groundwater flow, several simulated TDS profiles with depth at the end of the last glacial cycle will be compared to the observed profiles, as it was done in Section 6 for the last interglacial. The TDS data represent one of the few data sets available to validate the model at this scale. Figure 10 shows the simulated and observed TDS profiles in the Shield and in the Michigan basin. In the Canadian Shield as well as in the Michigan basin, the simulated results yield high concentrations at depth, but they fail to fit the observed data over the first 1000 m. In the upper 1000 m of the Shield, the observed TDS increases rapidly from a low concentration on the surface (10^2 mg/l) to about 10^5 mg/l at greater depths. As mentioned by *Lemieux et al.* [2008b], the freezing of water will expel TDS through salt rejection and consequently the ground ice will contain little salt. As a consequence, during a subsequent period of thaw, the TDS values would be low at shallow depths, noting that the permafrost usually forms within the upper 1000 m. Because salt rejection is not included in the model, the discrepancy between the observed and simulated TDS profiles is expected.

[51] Another explanation for the steep and uniform vertical TDS profiles computed by the model is because a large vertical transverse dispersivity, a value equal to 100 m, is used as input to describe the strength of the vertical mixing process. Such a value will promote strong vertical mixing, and hence high concentrations in the shallow groundwater; however, smaller values could not be used for the discretization used without introducing spurious numerical oscillations. While the discrepancy between the simulated and measured TDS profiles is of some concern at depths of less than 500 m, the agreement is very reasonable at larger depths because it captures the observed slope of the increase in TDS with depth.

[52] The impact of the ice sheet on continental groundwater flow over the full glacial cycle will first be examined at a randomly chosen observation point located in Timmins, Ontario, which is located in the Canadian Shield. At this location the vertical evolution of the groundwater flow system in response to the advance and retreat of the ice sheet will be described in detail. The location of the selected observation point is shown in Figure 4. Figure 11 shows the simulated hydraulic head and solute concentration at different depths along with the boundary conditions and climatic conditions applied on the surface over the glacial cycle.

[53] In order to visually illustrate the surface climatic conditions, a "climatic condition" graph is displayed on Figure 11a along with the applied boundary conditions at the surface of the flow model (Figure 11b). Above the horizontal line separating subglacial and periglacial conditions (Figure 11a), subglacial conditions prevail while periglacial conditions prevail below the line. The black

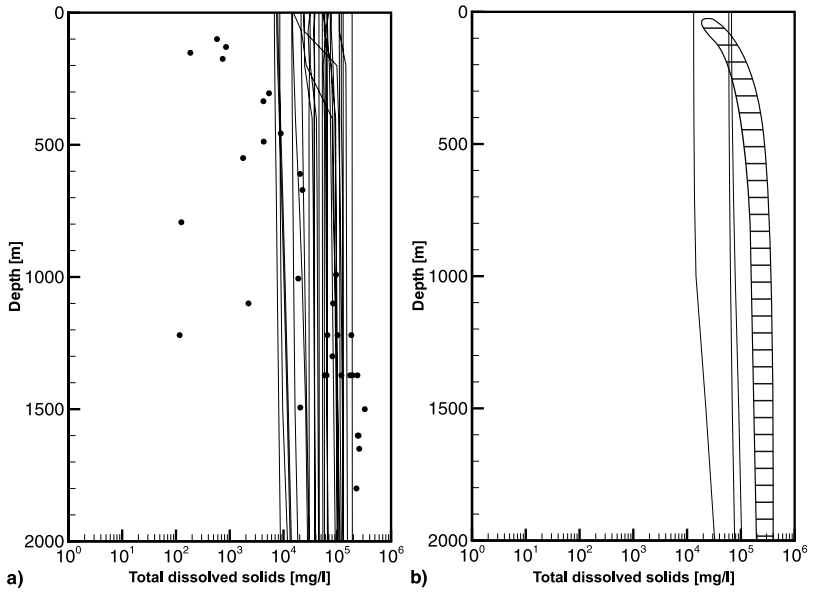

Figure 10. Simulated and observed total dissolved solids versus depth after the glacial cycle (0 ka) in (a) the Canadian Shield and (b) the Michigan Basin. Simulated TDS profiles are shown as continuous lines in both figures, and observed TDS profiles are shown as circles for the Canadian Shield and with a hatched zone for the Michigan Basin.

infilled region indicates that the subsurface is frozen and an unfilled box indicates frost-free conditions. For subglacial conditions, the bottom of the ice sheet can be warm based, meaning there is subglacial melting, or cold based, meaning there is no subglacial melting. For periglacial conditions, the water table can be at ground surface level, at a periglacial lake level or at sea level.

[54] Along with the climatic conditions graph, Figure 11b contains a summary of the surface boundary conditions applied at the observation locations. The ''elevation'' axis on the left is used to designate the value of several variables such as specified hydraulic head and permafrost depth. Other variables displayed are the ground surface elevation and ice sheet thickness. The summation of the ice sheet thickness and the ground surface elevation gives the ice sheet surface elevation. Permafrost thicknesses are shown as negative values to symbolize that it is progressing downward into the ground. The summation of the surface elevation and the permafrost thickness provides the elevation of the lower limit of the permafrost. Specified heads are designated using discrete symbols when this boundary condition is active in the model. A specified water flux, using values corresponding to the axis on the right, is prescribed when the specified head boundary condition is inactive and subglacial meltwater is being produced.

[55] At the observation point located near Timmins, Ontario (Figure 11), the impact of the three glacial advances on groundwater flow is clearly discernible. The last glacial advance is divided into two periods separated by a short interval of land exposure. The first glacial advance (−112 to −104 ka) produced a warm-based ice sheet over the period −110 to −105 ka (Figure 11a) during which there was meltwater production (Figure 11b). The magnitude of the groundwater velocity increases because of the infiltration of the subglacial meltwater (Figure 11d) and as a consequence, the solute concentration diminishes (Figure 11e). Note that spurious numerical oscillations occur at the land surface where the velocity is very high but they diminish soon after the sharp meltwater pulse terminates and the groundwater velocity returns to lower values. The hydraulic head increases by more than 1000 m near the surface but becomes constrained by the ice sheet thickness criterion. At depth, the head increases by a few hundred meters. The direction of the hydraulic gradient also reverses. Initially, the surface hydraulic head becomes higher than the head at depth as meltwater infiltrates into the subsurface but the opposite occurs when the ice retreats. After the retreat of the ice, the head stabilizes, as well as the concentration, and the permafrost returns to the land surface.

[56] At −71 ka, another glacial advance begins and, at −67 ka, the ice sheet becomes warm-based and meltwater production starts again. The meltwater dilutes the TDS and solute concentrations diminish while the hydraulic gradient is reversed from upward to downward. At the end of this second advance, the solute concentration (Figure 11e) rises slowly but diminishes rapidly shortly after the third glacial advance commences at −41 ka. The Darcy velocity magnitude peaks at about 4 mm/a, which is quite low compared to peak values in the sedimentary facies. Again, during most of the second glacial advance, the hydraulic head at the surface is constrained by the ice sheet thickness criterion because the bedrock cannot accommodate the subsurface drainage of all of the subglacial meltwater.

[57] After the ice retreat, the head on the surface returns to a value equal to the land surface elevation while the head is still quite high at depth (Figure 11c). The near-surface head then rises rapidly at the start of the third glacial advance (−41 ka), which produces a meltwater pulse that peaks at 4 cm/a. Then, depending on the rate of meltwater production, the solute concentration diminishes. Similar to

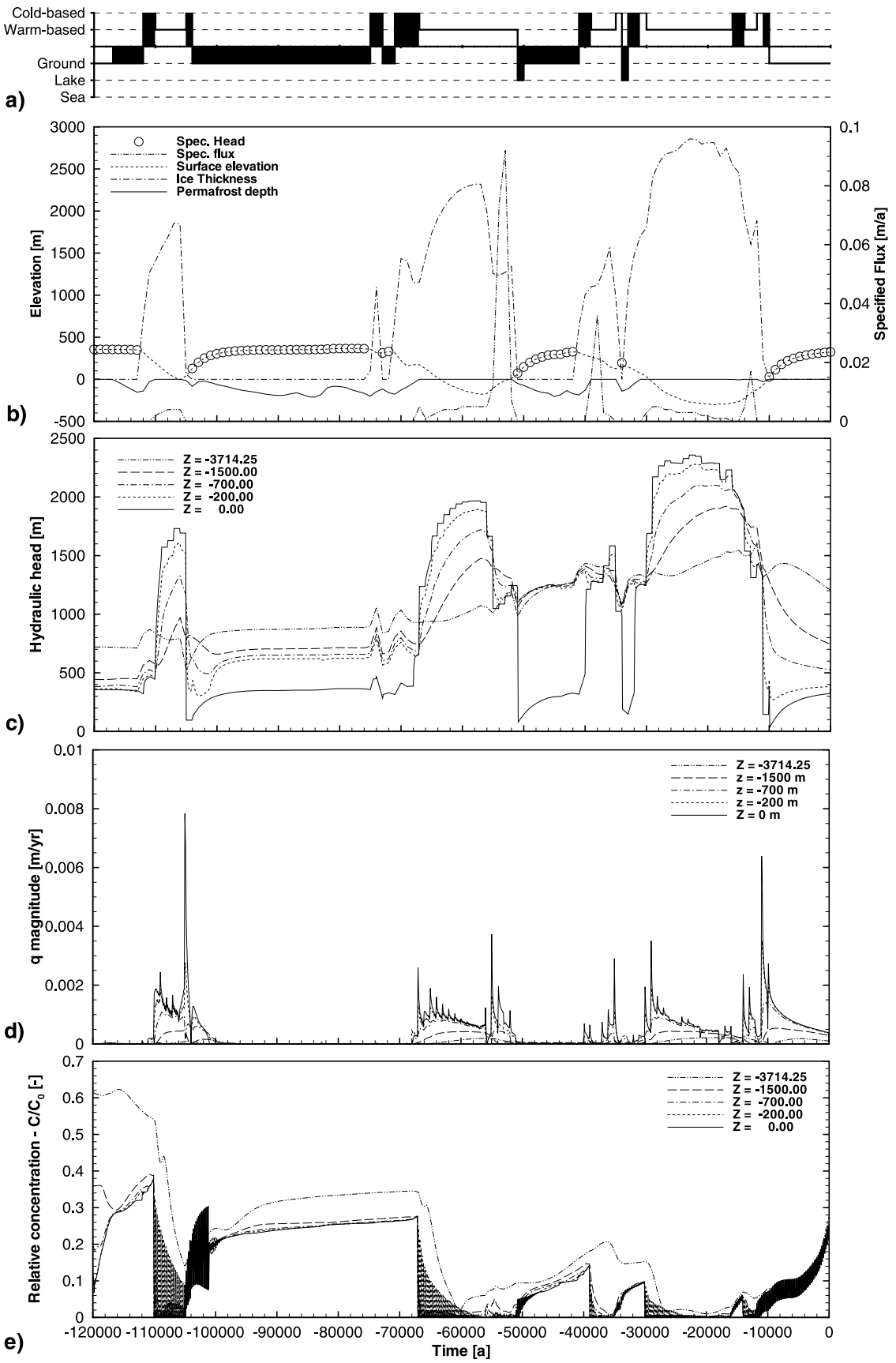

Figure 11. Observation point located at Timmins, Ontario, Canada measurements of (a) surface climatic conditions, (b) surface boundary conditions, (c) simulated hydraulic head, (d) simulated Darcy flux magnitude, and (e) simulated relative concentration (C/C_{max}).

the two previous ice advances, the hydraulic head at the surface is constrained by the ice sheet thickness. After the glacial maximum, the hydraulic head at all depths slowly returns to its original values; more rapidly near the surface, but slowly at depth. It can be seen that, at the end of the simulation, the head at depth has still not recovered to its original value. The concentration at the end of the simulation is also much lower at depth than it was originally.

[58] Additional insights pertaining to the impact of the Wisconsinian glaciation on continental groundwater flow can be gained by examination of the simulation results along a selected cross section. One vertical cross sections was extracted from the three-dimensional model to capture the hydraulic head response as affected by permafrost evolution and ice sheet loading at selected time slices (Figure 12). The location of the cross section is shown in Figure 4. In order to display the computed hydraulic heads and permafrost depths within the cross section as they evolve with time, time slices slightly before the LGM (−30 ka), at LGM (−20 ka), slightly after LGM (−14 ka) and finally at present time (0 ka) were selected. This succession of time slices sufficiently captures the impact of the ice sheet on groundwater flow. For illustrative purposes, the ice sheet thickness and its lateral extent is shown as the grey region on the top of the cross section.

[59] The rocks present over most of the cross section are the Shield rocks. The southern part of the cross section is located near Pittsburgh, PA, close to the Appalachian Mountains. The cross section then cuts across Lake Erie, Southwestern Ontario, Northern Ontario and then passes very close to the east of James and Hudson Bay, continuing north to the east of Baffin Island where it ends in the Arctic Ocean. In the northern part of the cross section, the ocean floor, whose elevation is at −600 m, represents about 20% of the section. The initial hydraulic head distribution at LIG exhibits a gravity-driven character with flow occurring from zones of high topography to regions of lower elevation (Figure 12a). Permafrost affects the near northern part of the section, although it disappears from the northern extremity of the section, under the Arctic Ocean. The maximum permafrost thickness reaches a depth of 600 m to 700 m.

[60] From the last interglacial at −120 ka to the first time slice at −30 ka, the ice sheet progressively migrated southward as well as the permafrost zone; the ice sheet covers the permafrost, however, as it advances. This situation is shown in Figure 12g. The thin layer of permafrost that was affecting the northern part of the cross section at LIG has melted almost completely as the ice sheet covered it at −30 ka. These windows of unfrozen materials allow the subglacial meltwater to infiltrate into the subsurface and increase the hydraulic head. The hydraulic head increases dramatically as the subglacial meltwater infiltrates into the subsurface (Figure 12b); the hydraulic head at a depth of up to 3000 m reaches a value of more than 1500 m under the main ice dome.

[61] At −20 ka, which is close to the last glacial maximum, the subglacial groundwater environment has further evolved and is less affected by the permafrost than it was at earlier times (Figures 12d and 12i). Most of the subglacial environment is open for subglacial meltwater infiltration and the hydraulic head increases consistently, which can be seen in all three cross sections. Consequently, with the penetration of subglacial meltwater into the subsurface, the solute concentration diminishes (Figure 11e). At this point, the groundwater flow patterns that are depicted on the two cross sections are drastically different than those of the last interglacial. This major difference is clear evidence of the large impact that the ice sheet had on groundwater flow.

[62] Following LGM, the ice sheet begins to retreat northward. At −14 ka, the groundwater flow system and solute concentration distribution are nevertheless similar to those existing at −20 ka; however, after about −14 ka, the ice sheet retreated rapidly and surface conditions changed dramatically. After the complete retreat of the ice (0 ka), it can be seen on each cross section that the high hydraulic heads that developed at depth under the ice sheet have diminished although the values are higher than at LIG. Several overpressurized zones can be seen at depth and occasionally near the surface (Figure 12e). The reason for the existence of the shallow zones of high pressures is because the permafrost reappeared on the surface, after the glacial retreat, before the high hydraulic heads could dissipate (Figures 12e and 12j).

9. Permafrost Impact on the Groundwater Flow System

[63] In order to capture the importance of permafrost on the evolution of the groundwater flow system during the last glacial cycle, the base case scenario was modified to neglect the existence of permafrost. One striking aspect of the simulation results, however, is that the neglect of the permafrost does not appear to significantly modify the flow system during the glacial cycle. This can be seen by comparing Figures 13 (no permafrost) and 12 (with permafrost). Because the permafrost acts like a barrier to surface/subsurface water interaction, it would have been expected that its neglect would have exposed a much larger area for subglacial meltwater infiltration, and therefore significantly increased the infiltration. It was shown by *Lemieux et al.* [2008a], however, that infiltration does not increase when the permafrost is neglected. The glacial systems model (which ignores possible englacial transport of surface melt) requires warm-based ice to produce subglacial meltwater. Warm-based ice is generally incompatible with near-surface permafrost. Therefore, even if the permafrost is neglected, there is little or no subglacial meltwater available to infiltrate into the subsurface.

[64] It was shown on Figure 12e that, at the end of the simulation period, the permafrost had trapped a high-pressure zone at depth because it could not dissipate by vertical flow to the surface where the head is lower. It can be seen by comparing Figure 13e (no permafrost) with Figure 12e (with permafrost) that, although an overpressurized zone remains at depth for the no permafrost case, it has a lower peak and high heads are not trapped near the surface. The occurrence of a trapped high-pressure zone below the permafrost at the end of the glacial cycle highlights the importance of the permafrost to control the recovery of the flow system after a glacial cycle. The presence of taliks, as currently observed at high latitudes, might dissipate the high-pressure zones locally; their inclusion in a model may therefore be important at a subregional

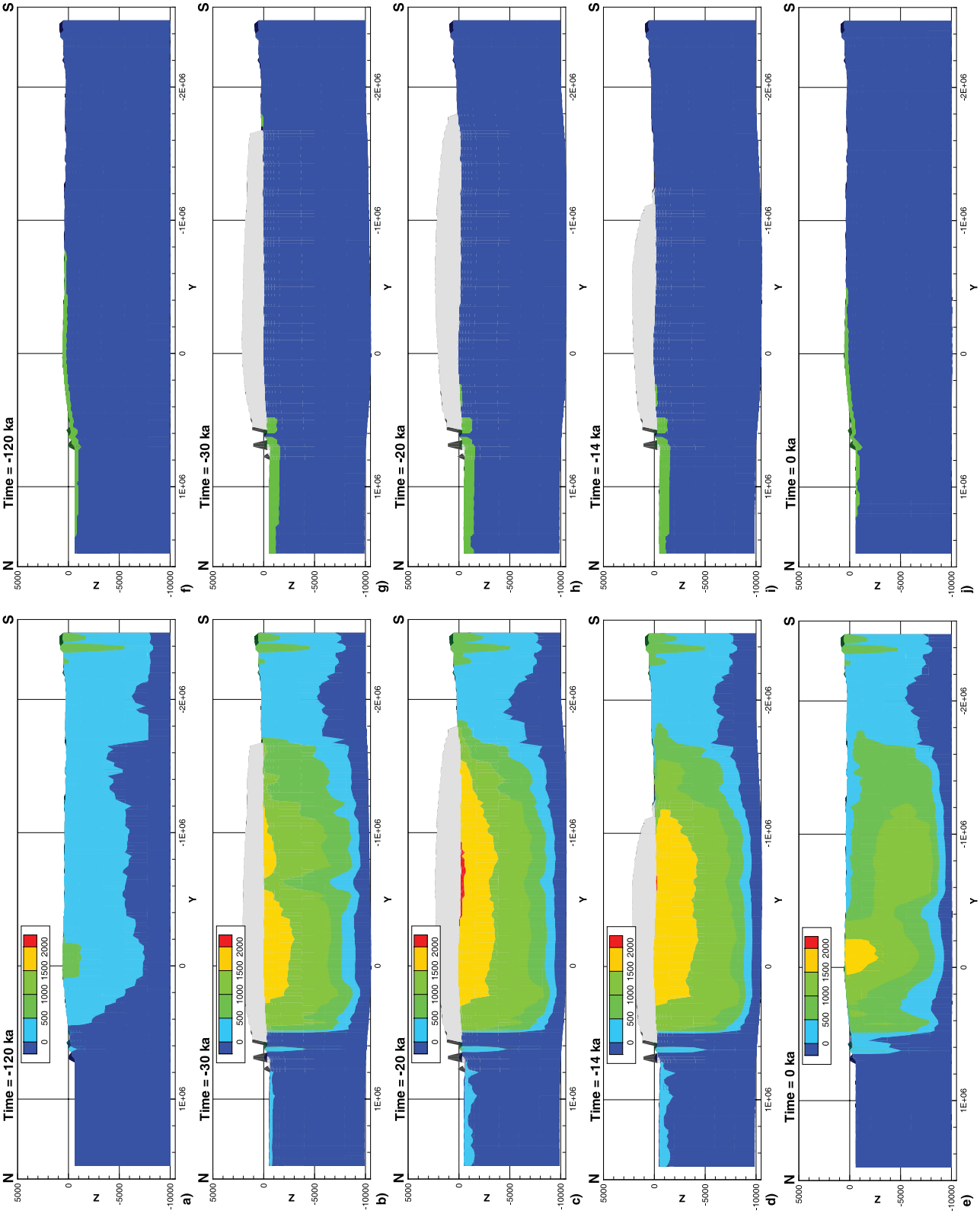

Figure 12. Hydraulic head and permafrost along a north-south cross section shown in Figure 4 at (a and f) −120, (b and g) −30, (c and h) −20, (d and i) −14, and (e and j) 0 ka. Vertical exaggeration is 100×.

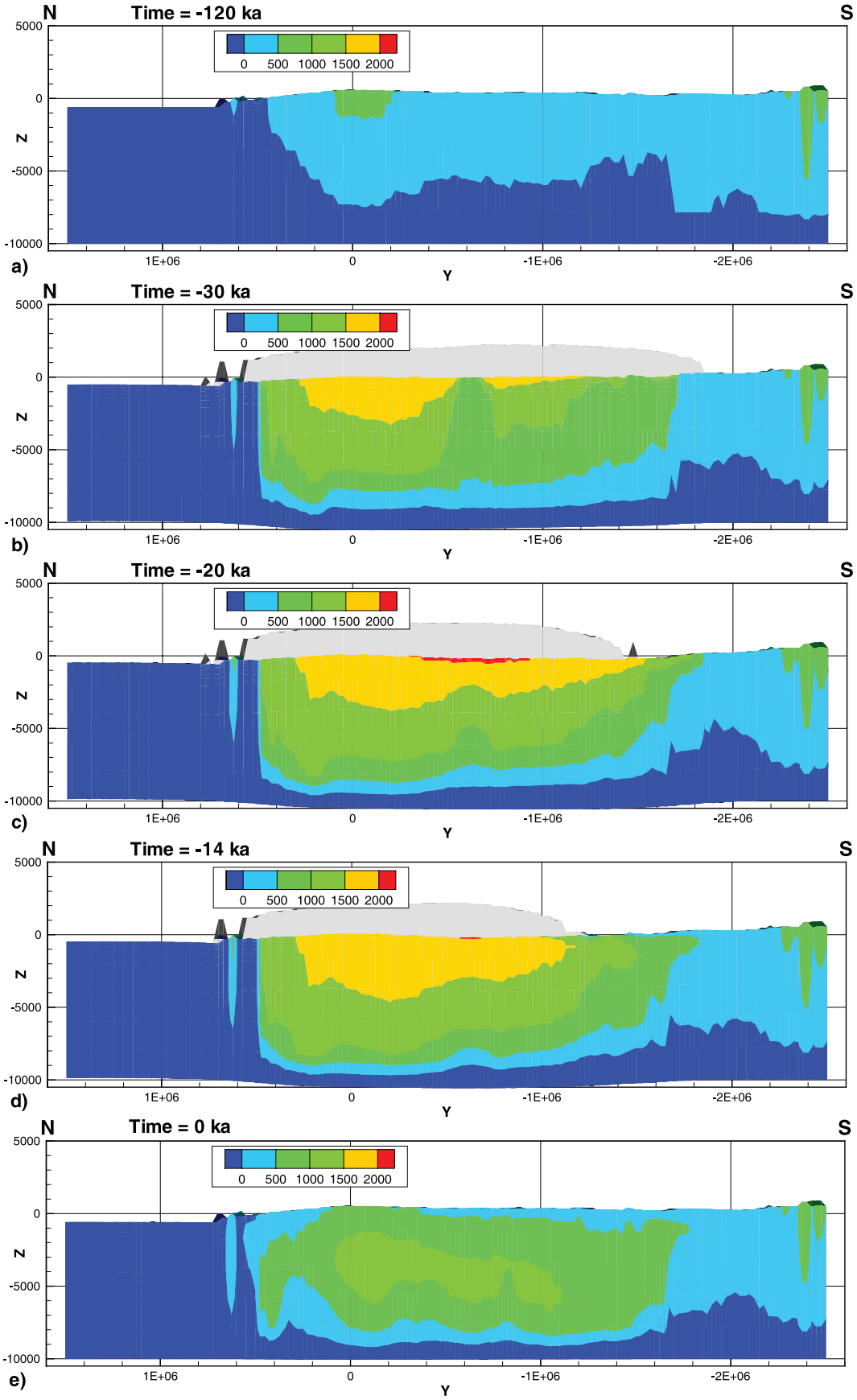

Figure 13. Hydraulic head for a case neglecting permafrost north-south cross section shown in Figure 4 at selected time slices: (a) −120, (b) −30, (c) −20, (d) −14, and (e) 0 ka. Vertical exaggeration is 100×.

scale in order to correctly reproduce observed hydraulic head patterns.

10. Limitations

[65] Although several key factors related to the impact of glaciation on continental groundwater flow were highlighted, the scale and complexity of the model brings to bear some limitations that should be recognized. First, the geological model used to assign the subsurface hydraulic properties is quite simple and does not include local and regional heterogeneities. For example, the sedimentary basins, which include both high- and low-permeability strata could not be discretized due in part to the relatively small size of the individual formations compared to the size of the entire model, but also because of the paucity of high-resolution 3-D stratigraphic data covering the entire continent. Basic regional flow trends are, however, believed to be captured by the model. Other aspects not included in the flow model include major faults and hydraulic anisotropy.

[66] Permafrost formation creates several consequences that are not represented in the numerical model because of their complexity. Salt rejection upon the freezing of water is one of the processes thought to be important. *Starinsky and Katz* [2003], for example, hypothesized that this phenomenon is responsible for the formation of the Shield brines, although their hypothesis remains contentious. The migration of dissolved salts downward with the advance of the permafrost front would increase the water density at depth. During the thawing of the permafrost zone, low TDS water would exist at shallow depths at least until upward migration of the TDS occurs via diffusion and any upward advection that develops.

[67] The relative permeability of permafrost to ice content is another area that could benefit from additional laboratory and field measurements. Pore water expulsion due to volume expansion during freezing is yet another process that is not well documented in the literature [*Anderson and Morgenstern*, 1973]. The inclusion of these phenomena into a numerical model is a formidable task especially if it is desired to account for the consequences in the context of a regional- or continental-scale model.

[68] Another uncertain aspect in the model concerns the initial condition in the subsurface. Because there are no exhaustive paleohydrogeological data available at the continental scale, the model was executed until a steady state was achieved using the LIG boundary conditions in order to obtain the initial conditions for the transient glacial cycle simulations. In the future, it would be best to start the model from equilibrium and run it through a few glacial cycles to come up with a better set of initial conditions for the LIG. Nevertheless the methodology used here yields reasonable results for the TDS profiles across the Shield and the Michigan basin, but other benchmark measurements such as ^{14}C age dating of the subsurface pore waters at various depths and locations would greatly improve confidence in the model.

[69] Finally, a more detailed representation of sedimentary basins would allow the use of documented pore pressure as another calibration data set and possibly explain some anomalous pore pressure measurements. For example, *Bahr et al.* [1994] presents anomalous pore pressure data up to 250 m for confining units within the Michigan basin. These have never been adequately explained. Comparable anomalous pore pressure data exists for the Western Canadian Basin [*Bekele et al.*, 2003].

11. Summary

[70] In this paper, an externally forced, fully transient groundwater flow model accounting for density-dependant solute transport was used to address the impact of the Wisconsinian glaciation on continental groundwater flow in three dimensions over the Canadian landscape. The simulated TDS concentrations were compared to currently available TDS observations. Although the general trend of the increase in concentration values at depth is captured, the model differences occur at shallow depths. It is believed that inclusion of the phenomenon of salt expulsion from freezing water in the model during permafrost penetration and the use of smaller vertical dispersivity value would ameliorate this discrepancy.

[71] During the last glacial cycle, the ice sheet advanced and retreated several times to form three local glacial maxima. Each of these glacial advances had a different impact on groundwater flow because of their different intensities and durations. Their relative impact on flow system behavior follows the same sequence as their timing, with the first being the least important and the last one being the most significant. The last glacial advance was of the longest duration and produced the thickest ice sheet.

[72] The impact of the ice sheet on groundwater flow was shown to be dramatic. Hydraulic head values below the ice sheet increased by as much as 3000 m down to a depth of 1.5 km into the subsurface. At present time, large overpressurized zones should still be observed at depth because very long time frames are required to dissipate the large pressures at large depths. The increase in the hydraulic head is attributed to the infiltration of subglacial meltwater into the rocks and because of the surface loading induced by the ice sheet. During a glacial cycle, vertical hydraulic gradients can reverse depending on the location relative to the ice sheet margin, and the magnitude of the Darcy flux can vary in time by as much as 2 orders of magnitude at depths of 700 m and greater. The distribution of the TDS concentrations were highly modified and large lenses of reduced concentration appeared at some locations. This arose from pulses of low TDS subglacial meltwater that infiltrated to depths greater than a kilometer in some areas.

[73] The neglect of permafrost in the model does not appear to significantly modify the flow system during the glacial cycle, at least in subglacial zones. This is because subglacial regions affected by permafrost do not produce meltwater and therefore, when the permafrost is ignored, no change in subglacial infiltration occurs. On the other hand, permafrost has a large impact on the rate of dissipation of high hydraulic heads that build at depth as a consequence of subglacial infiltration and ice loading; the permafrost forms a cap on the surface which inhibits the pressure dissipation process. The occurrence of a trapped pressure zone below the permafrost after a glacial cycle highlights the importance of the permafrost distribution on the recovery of the flow system. The presence of taliks, as currently observed at

high latitudes, could enhance the rate of dissipation of these high pressure zones in the model.

[74] On the basis of the hydraulic head and TDS concentration results after the last glacial cycle, it was shown that the flow system did not fully revert to its initial LIG condition, and that it is still recovering from the LGM perturbation. This suggest that the current groundwater flow system cannot be interpreted solely on the basis of present-day boundary conditions and it is likely that several thousands of years of additional equilibration time will be necessary for the system to reach a new quasi-steady state. This further invalidates the assumption of a steady state to simulate a time slice of the impact of glaciation on large-scale groundwater flow.

[75] **Acknowledgments.** Financial support for this study was provided by the Natural Sciences and Engineering Research Council of Canada (NSERC) and the Ontario Graduate Scholarship (OGS) program as scholarships to J.-M. Lemieux and also from NSERC and the Canada Research Chairs program as research funding to E.A. Sudicky. We would like to thank Ingrid Stober and Kurt Bucher for granting permission to reproduce and modify Figure 2. The authors thank Grant Ferguson for carefully reviewing the three papers related to this work. We also appreciated the constructive reviews of Volker Rath, Mark Person, and the associate editor whose comments greatly helped improving the original manuscript.

References

Anderson, D. M., and N. R. Morgenstern (1973), Physics, chemistry and mechanics of frozen ground: A review, in *Proceedings of 2nd International Conference on Permafrost, North American Contributions, Yakutsk, USSR*, pp. 257–288, Natl. Acad. of Sci., Washington, D. C.

Bahr, J. M., G. R. Moline, and G. Nadon (1994), Anomalous pressures in the deep Michigan Basin, in *Basin Compartments and Seals, Am. Assoc. Pet. Geol. Mem. Ser.*, vol. 61, edited by P. Ortoleva, pp. 153–165, Am. Assoc. of Pet. Geol., Tulsa, Okla.

Bekele, E. B., B. J. Rostron, and M. A. Person (2003), Fluid pressure implications of erosion unloading, basin hydrodynamics and glaciation in the Alberta Basin, *J. Geochem. Explor.*, *78–79*, 143–147.

Dollar, P., S. K. Frape, and R. H. McNutt (1991), Geochemistry of formation waters, southwestern Ontario, Canada and southern Michigan, U. S. A.: Implications for origin and evolution, *Open File Rep. 5743*, 72 pp., Ont. Geol. Surv., Toronto, Ont., Canada.

Domenico, P. A., and G. A. Robbins (1985), The displacement of connate water from aquifers, *Geol. Soc. Am. Bull.*, *96*(3), 328–335.

Douglas, R. J. W. (1970), Introduction, in *Geology and Economic Minerals of Canada*, Econ. Geol. Rep., vol. 1, 5th ed. edited by R. J. W. Douglas, 838 pp., Geol. Surv. of Can., Ottawa, Ont.

Farvolden, R. N., O. Pfannkuch, R. Pearson, and P. Fritz (1988), Region 12: Precambrian Shield, in *Hydrogeology*, edited by W. Back, J. S. Rosenhein, and P. R. Seaber, pp. 101–114, Geol. of N. Am., Boulder, Colo.

Ferguson, G. A. G., R. N. Betcher, and S. E. Grasby (2007), Hydrogeology of the Winnipeg Formation in Manitoba, Canada, *Hydrogeol. J.*, *15*, 573–587, doi:10.1007/s10040-006-0130-4.

Fisher, A. T. (1998), Permeability within basaltic oceanic crust, *Rev. Geophys.*, *32*(2), 142–182.

Foxworthy, B. L., D. L. Hanneman, D. L. Coffin, and E. C. Halstead (1988), Region 1: Western mountain ranges, in *Hydrogeology*, edited by W. Back, J. S. Rosenhein, and P. R. Seaber, pp. 25–35, Geol. of N. Am., Boulder, Colo.

Frape, S. K., and P. Fritz (1987), Geochemical trends for groundwaters from the Canadian Shield, in *Saline Water and Gases in Crystalline Rocks*, *Geol. Assoc. Can. Spec. Pap.*, vol. 33, edited by P. Fritz and S. K. Frape, pp. 19–38, Geol. Assoc. of Can., St. John's, Newfoundland and Labrador, Canada.

Freeze, R. A., and P. A. Witherspoon (1967), Theoretical analysis of regional ground-water flow: 2. Effect of water-table configuration and subsurface permeability variations, *Water Resour. Res.*, *3*(2), 623–634.

Frost, L. H. (1997), Underground Research Laboratory shaft excavation drawdown experiment: Estimate of hydraulic parameter values for moderately fractured rock, *Tech. Rep. TR-751 COG-96-282-I*, At. Energy of Can. Ltd., Pinawa, Manit., Canada.

Frost, L. H., and R. A. Everitt (1997), Excavation damage zone tracer experiment in the floor of the room 415 test tunnel, *Tech. Rep. AECL-11640 COG-96-321-I*, At. Energy of Can. Ltd., Pinawa, Manit., Canada.

Garven, G. (1989), A hydrogeologic model for the formation of the giant oil sands deposits of the western Canada sedimentary basin, *Am. J. Sci.*, *289*, 105–166.

Garven, G. (1995), Continental-scale groundwater flow and geologic processes, *Annu. Rev. Earth Planet. Sci.*, *23*, 89–117.

Gascoyne, M., and M. I. Sheppard (1993), Evidence of terrestrial discharge of deep groundwater on the Canadian Shield from helium in soil gases, *Environ. Sci. Technol.*, *27*(12), 2420–2426.

Globensky, Y. (1987), Géologie des basses-terres du Saint-Laurent, *Tech. Rep. MM 85-02*, Minist. de l'Énergie et des Ressour., Québec, Que., Canada.

Grasby, S., K. Osadetz, R. Betcher, and F. Render (2000), Reversal of the regional-scale flow system of the Williston basin in response to Pleistocene glaciation, *Geology*, *28*(7), 635–638.

Grasby, S. E., and R. N. Betcher (2002), Regional hydrogeochemistry of the carbonate rock aquifer, southern Manitoba, *Can. J. Earth Sci.*, *39*(7), 1053–1063.

Grasby, S. E., and Z. Chen (2005), Subglacial recharge into the western Canada sedimentary basin—Impact of Pleistocene glaciation on basin hydrodynamics, *Geol. Soc. Am. Bull.*, *117*(3–4), 500–514.

Hubbert, M. K. (1940), The theory of groundwater motion, *J. Geol.*, *48*, 785–944.

Huenges, E., J. Erzinger, J. Kück, B. Engeser, and W. Kessels (1997), The permeable crust: Geohydraulic properties down to 9101 m depth, *J. Geophys. Res.*, *102*(B8), 18,255–18,265.

Ingebritsen, S. E., and C. E. Manning (1999), Geological implications of a permeability-depth curve for the continental crust, *Geology*, *27*(12), 1107–1110.

Ingebritsen, S. E., and W. E. Sanford (1998), *Groundwater in Geologic Processes*, Cambridge Univ. Press, New York.

Kuchling, K., D. Chorley, and W. Zawadski (2000), Hydrogeological modeling of mining operations at the Diavik Diamonds project, in *Environmental Issues and Management of Waste in Energy and Mineral Production: Proceedings of the Sixth International Symposium, Calgary, Alberta, Canada, 30 May–2 June 2000*, A.A. Balkema, Rotterdam, Netherlands.

Lemieux, J.-M., R. Therrien, and D. Kirkwood (2006), Small scale study of groundwater flow in a fractured carbonate-rock aquifer at the St-Eustache Quarry, Québec, Canada, *Hydrogeol. J.*, *14*(3), 603–612, doi:10.1007/s10040-005-0457-2.

Lemieux, J.-M., E. A. Sudicky, W. R. Peltier, and L. Tarasov (2008a), Dynamics of groundwater recharge and seepage over the Canadian landscape during the Wisconsinian glaciation, *J. Geophys. Res.*, *113*, F01011, doi:10.1029/2007JF000838.

Lemieux, J.-M., E. A. Sudicky, W. R. Peltier, and L. Tarasov (2008b), Simulating the impact of glaciations on continental groundwater flow systems: 1. Relevant processes and model formulation, *J. Geophys. Res.*, doi:10.1029/2007JF000928, in press.

Manning, C. E., and S. E. Ingebritsen (1999), Permeability of the continental crust: Implications of geothermal data and metamorphic systems, *Rev. Geophys.*, *37*(1), 127–150.

McIntosh, J. C., and L. M. Walter (2005), Volumetrically significant recharge of Pleistocene glacial meltwaters into epicratonic basins: Constraints imposed by solute mass balances, *Chem. Geol.*, *222*(3–4), 292–309.

Nastev, M., M. M. Savard, P. Lapcevic, R. Lefebvre, and R. Martel (2004), Hydraulic properties and scale effects investigation in regional rock aquifers, south-western Quebec, Canada, *Hydrogeol. J.*, *12*(3), 257–269.

Neuzil, C. E. (1995), Abnormal pressures as hydrodynamic phenomena, *Am. J. Sci.*, *295*, 742–786.

Provost, A. M., C. I. Voss, and C. E. Neuzil (1998), Glaciation and regional ground-water flow in the Fennoscandian Shield: Site 94, *SKI Rep. 96:11*, Swed. Nucl. Power Insp., Stockholm.

Randall, A. D., R. M. Francis, M. H. Frimpter and J. M. Emery (1988), Region 19: Northeastern Appalachians, in *Hydrogeology*, edited by W. Back, J. S. Rosenhein, and P. R. Seaber, pp. 177–187, Geol. of N. Am., Boulder, Colo.

Raven, K. G. (1986), Hydraulic characterization of a small groundwater flow system in fractured monzonitic gneiss, *Natl. Hydrol. Res. Inst. Pap. 30/Inland Waters Dir. Ser. 149*, Environ. Can., Ottawa, Ont.

Raven, K. G., and J. E. Gale (1986), A study of the surface and subsurface conditions at selected underground mines and excavations, *Tech. Rep. TR-177*, At. Energy of Can. Ltd., Pinawa, Manit., Canada.

Raven, K. G., D. J. Bottomley, R. A. Sweezey, J. A. Smedley, and T. J. Ruttan (1987), Hydrogeological characterization of the East Bull Lake research area, *Natl. Hydrol. Res. Inst. Pap. 31/Inland Waters Dir. Ser. 160*, Environ. Can., Ottawa, Ont.

Rouleau, A., J. Guha, G. Archambault, and A. Benlahcen (2003), An overview of the hydrogeology of the Precambrian basement in Quebec and related mining problems, in *Proceedings of the International Conference on Groundwater in Fractured Rocks, Prague, Czech Republic, 15–19*

September 2003: Extended Abstracts, edited by J. Krásny, Z. Hrkal, and J. Bruthans, pp. 379–380, U. N. Educ. Sci. and Cult. Organ., Paris.

Sheppard, M. I., D. H. Thibault, G. M. Milton, J. A. K. Reid, P. A. Smith, and K. Steve (1995), Characterization of a suspected terrestrial deep groundwater discharge area on the Canadian Precambrian shield, *J. Contam. Hydrol.*, *18*(1), 59–84.

Spencer, R. J. (1987), Origin of Ca-Cl brines in Devonian formations, western Canada sedimentary basin, *Appl. Geochem.*, *2*(2), 373–384.

Starinsky, A., and A. Katz (2003), The formation of natural cryogenic brines, *Geochim. Cosmochim. Acta*, *67*(8), 1475–1484.

Stevenson, D. R., A. Brown, C. C. Davison, M. Gascoyne, R. G. McGregor, D. U. Ophori, N. W. Scheier, F. Stanchell, G. A. Thorne, and D. K. Tomsons (1996), A revised conceptual hydrogeologic model of a crystalline rock environment, Whiteshell research area, southeastern Manitoba, Canada, *Tech. Rep. AECL 11331 COG-95-271*, At. Energy of Can. Ltd., Pinawa, Manit., Canada.

Stober, I., and K. Bucher (2004), Fluid sinks within the Earth's crust, *Geofluids*, *4*(2), 143–151.

Stober, I., and K. Bucher (2005), The upper continental crust, an aquifer and its fluid: Hydaulic and chemical data from 4 km depth in fractured crystalline basement rocks at the KTB test site, *Geofluids*, *5*(1), 8–19.

Tarasov, L., and W. R. Peltier (2004), A geophysically constrained large ensemble analysis of the deglacial history of the North American ice-sheet complex, *Quat. Sci. Rev.*, *23*(3–4), 359–388.

Tóth, J. (1962), A theory of ground-water motion in small drainage basins in central Alberta, Canada, *J. Geophys. Res.*, *67*(11), 4375–4387.

Tóth, J. (1963), A theoretical analysis of groundwater flow in small drainage basins, *J. Geophys. Res.*, *68*(10), 4795–4812.

Wheeler, J. O., P. F. Hoffman, K. D. Cardand, A. Davidson, B. V. Sanford, A. V. Okulitch, and W. R. Roest (1997), Geological map of Canada, *Map D1860A*, Geol. Surv. of Can., Ottawa, Ont.

J.-M. Lemieux and E. A. Sudicky, Department of Earth and Environmental Sciences, University of Waterloo, Waterloo, ON, Canada N2L 3G1. (jmlemieux@alumni.uwaterloo.ca; sudicky@sciborg.uwaterloo.ca)

W. R. Peltier, University of Toronto, Department of Physics, 60 St. George Street, Toronto, ON, Canada M5S 1A7. (peltier@atmosp.physics.utoronto.ca)

L. Tarasov, Department of Physics and Physical Oceanography, Memorial University of Newfoundland, St. John's, NL, Canada A1C 5S7. (lev@physics.mun.ca)